Delayed hadrons in extensive air showers: Evidence for the iron-group nuclei in primary cosmic-ray flux at energies $\sim 10^{13}-10^{15}$ eV

J. A. Goodman, R. W. Ellsworth,* A. S. Ito,† J. R. MacFall,‡ F. Siohan,§
R. E. Streitmatter,|| S. C. Tonwar,¶ P. R. Viswanath,** and G. B. Yodh
Department of Physics and Astronomy, University of Maryland, College Park, Maryland 20742
(Received 6 April 1982)

The distribution of arrival time of energetic hadrons in the near-core region of air showers of energies $\sim 10^4-10^6$ GeV relative to the shower front has been studied experimentally at mountain altitude. The observed rate of hadron events with (i) energy >50 GeV in the calorimeter, (ii) associated shower particle density >18 m^{-2}, and (iii) a signal ≥ 5 equivalent particles in a plastic scintillator T_3 of area 0.54 m^2 placed under 220 g cm^{-2} of absorber in the calorimeter is found to be 1.85×10^{-3} m^{-2}sr^{-1}sec^{-1}. Of these events a fraction $(0.55\pm 0.05)\%$ have shown the signal from T_3 to be delayed by 15 nsec or greater relative to shower particles. Monte Carlo simulations of experimental observations have shown that these requirements on energy and shower density enhance the sensitivity of the observed rate to the contributions due to showers initiated by heavy nuclei. Calculations also show that observed delayed hadrons are mostly associated with showers due to heavy nuclei. For interpretation of observed features two models for primary composition have been considered. In the first model the power-law spectra for protons and lighter nuclei are assumed to have spectral index γ_p and the heavy (iron group) nuclei the index γ_{Fe}. An agreement between the expectation and observation requires the values of γ_p and γ_{Fe} to be significantly different as -2.68 and -2.39 in the energy range $\sim 10^3-10^6$ GeV. In the second model the spectral index γ is assumed to be the same for all components and the spectra steepen by 0.5 at the same rigidity R_c. It is found that the values of γ and R_c should be -2.55 and 10^5 GV/c, respectively, to match the observations. It is concluded that a successful understanding of experimental observations requires a relative change between the energy spectra of protons and heavy nuclei in the energy range $\sim 10^4-10^6$ GeV, which would make the proportion of iron-group nuclei about 40% of the primary flux at these energies.

I. INTRODUCTION

The elemental composition of primary cosmic rays at high energies plays a crucial role in the development of extensive air showers in the atmosphere. A knowledge of the energy spectra of various components of primary cosmic rays at air-shower energies is therefore very essential for successful interpretation of many observations on various components of air showers. This information is also needed for a better understanding of the acceleration mechanisms and the nature of sources producing high-energy cosmic rays. Direct measurements[1,2] of the energy spectra for various nuclei have been done using a variety of particle detectors carried by balloons and satellites. However, practical limitations imposed on the weight of the detectors and possible exposure times have prevented experimenters from obtaining direct information about elemental composition above energies of a few hundred GeV per nucleon. Although the pioneering experiments by Grigorov *et al.*[1] were successful in measuring the energy spectrum of all particles over a broad energy interval ($\sim 10^2$ to 10^5 GeV per nucleus), their measurements of composition were affected by back-scattered particles[3] from interactions in the calorimeter. Experimental observations of electron and muon components of air showers initiated by primaries of energies $\sim 10^5-10^8$ GeV have been interpreted[4,5] to suggest that heavy nuclei (mainly iron group) form a significant part of the primary flux at these energies. However, this interpretation is dependent on the assumed characteristics of particle interactions at energies of 10^6-10^8 GeV and is applicable only if scaling[6,7] is not grossly violated. In fact some of these observations have also been interpreted[8] to indicate violation of scaling behavior in high-energy particle interactions at energies above 10^5 GeV. It is therefore of great interest to study other parame-

ters of air showers which also depend sensitively on the atomic mass of the primaries. A study of small-size showers of energies $\sim 10^5 - 10^6$ GeV is to be preferred for this purpose in order to reduce the uncertainties due to extrapolation of particle-interaction characteristics to higher energies. Also, detailed information on particle interactions for equivalent laboratory energies up to $\sim 1.5 \times 10^5$ GeV will become available in the near future from experiments now being carried out at the CERN $\bar{p}p$ collider facility. Preliminary results available from these experiments[9] already suggest that scaling is violated only mildly in the central region at these high energies.

Monte Carlo simulations of air showers using a scaling model have shown[10] that one of the experimentally observable parameters which is very sensitive to the atomic mass of the primaries is the number of delayed hadrons detected near the core region of air showers. We have studied experimentally the arrival-time distribution of hadrons near air-shower cores and have already reported some of our preliminary results.[11,12] These results, based on a comparison of observations with expectations from Monte Carlo simulations, have shown that the iron-group nuclei become a significant component of the primary-cosmic-ray flux at energies $\sim 10^5 - 10^6$ GeV/nucleus. We have now completed the analysis of the experimental data and have carried out more detailed simulation of air showers for comparison with this data including a realistic simulation of the experimental system. In this paper the details of the experiment are reported in Sec. II and the experimental results are discussed in Sec. III. The details of the simulation procedure and the assumptions underlying the generation of hadron and electron-photon cascades in the atmosphere and in the calorimeter are given in Sec. IV. A comparison of the experimental results with the expectations from simulation is given in Sec. V. The results obtained from this analysis along with results given by other related experiments are discussed in Sec. VI. The sensitivity of results to scaling violations is also discussed in this section. Finally, the conclusions about the primary-cosmic-ray composition drawn from this study are presented in the last section.

II. EXPERIMENTAL DETAILS

The experiment was carried out at the Sacramento Ridge Cosmic Ray Laboratory, Sunspot (altitude 2900 m, 730 g cm^{-2}) in New Mexico. Data were collected during the period April 1975 to May 1976.

A. Apparatus

The experimental system, shown schematically in Fig. 1 basically consists of a shower-detection array and a calorimeter. Four detectors T_{1E}, T_{1W}, D_1, and D_2 form the shower-detection system and measure the shower density and its arrival time. The detectors T_{1E} and T_{1W} are plastic scintillators, each of dimension 0.9×1.8 m $\times 1.2$ cm, viewed on both ends with fast photomultipliers (56 AVP). These are located above the calorimeter and provide the time reference for measuring the arrival delay of hadrons interacting in the calorimeter. The other shower detectors D_1 and D_2 are liquid scintillators (0.7 m $\times$ 0.7 m $\times$ 0.1 m) viewed from above by fast photomultipliers. These detectors were placed at a distance of 3 m from the center of the calorimeter on opposite corners. The calorimeter[13] with a cross-sectional area of 2.29×2.13 m^2 and a depth of 985 g cm^{-2} of iron ($\sim 8\lambda_p$ or ~ 66 radiation lengths) had seven detector layers for sampling the ionization produced by particles generated in the hadron-electron-photon cascade. Two liquid-scintillator tanks, each of area 2 m $\times$ 1 m and viewed by six photomultipliers (RCA 6655), were placed side by side to form a detector layer. Inside the calorimeter, at a depth

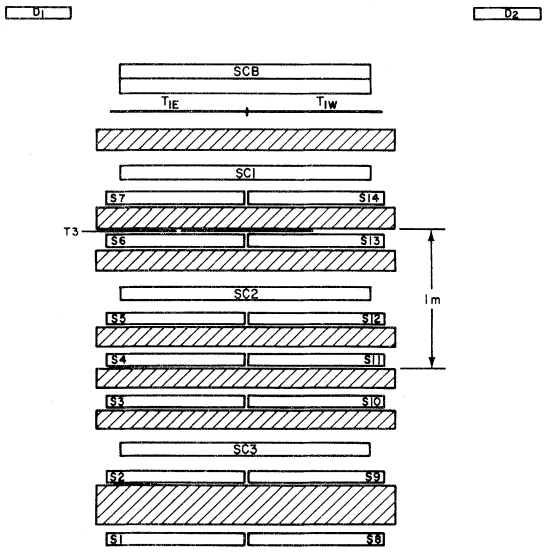

FIG. 1. A schematic diagram of the experimental system showing the relative positions of liquid-scintillation tanks, shower detectors, hadron detector, and spark chambers in the calorimeter.

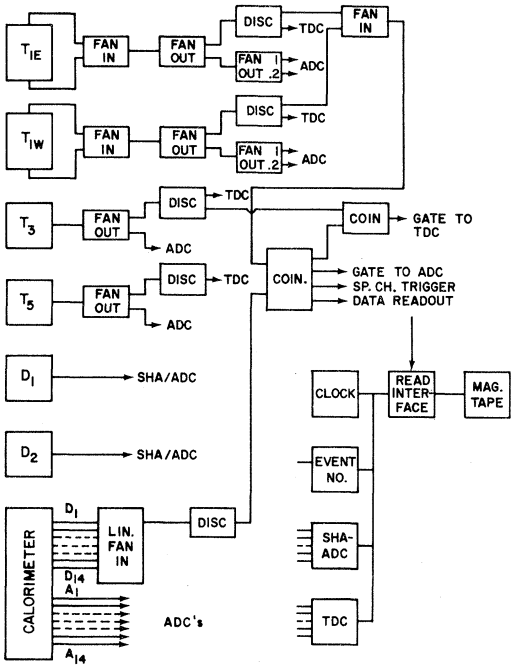

FIG. 2. A schematic diagram of data selection and recording system.

of 220 g cm^{-2} of iron, a plastic scintillation counter T_3 (0.9 m$\times$0.6 m$\times$1.2 cm) was placed to measure the arrival time of the hadrons. For part of the experiment another scintillation detector T_5, of the same area as T_3, was placed right above T_3, to estimate the fluctuations in pulse heights obtained from T_3. Four wide-gap spark chambers were used to obtain visual information on the shower and the hadron cascade. Three of these chambers, SC1, SC2, and SC3 (each 1.8 m$\times$1.8 m$\times$12.5 cm) were located at different depths inside the calorimeter as shown in Fig. 1. The fourth chamber SCB, with a double gap, was located above the calorimeter. The spark chambers were fired with a delay of 1 μsec to eliminate unwanted noise in the detectors and electronics. Absence of interference from noise was ensured from a comparison of data taken with and without spark chambers. A stack of 24 proportional chambers (each 1 m^2 in area) with styrofoam radiators sandwiched between them was located above the beam chamber. It was used to measure transition radiation[14] emitted by very-high-energy unaccompanied hadrons for distinguishing between pions and protons. However, since the information from this detector system has not been used in this experiment, it is not shown in Fig. 1. The absorber thickness offered by the transition-radiation detector was rather small ($\sim$5 g cm^{-2}) and need not be considered in the present study.

B. Event selection and recording

Main features of the selection and data-recording system relevant to the present experiment are shown schematically in Fig. 2. The anode pulses from the photomultipliers viewing the scintillator T_{1E} (and separately T_{1W}) were summed through a passive summing device (fan-in). This sum pulse was fed after a passive splitting to a discriminator and after further splitting to two channels of the sample-and-hold-amplifier—analog-to-digital-converter (SHA-ADC) system (LRS 227—LRS 243). One of these inputs to SHA was attenuated by a factor of 5 to extend the range of measurement of pulse amplitude from the detector. One of the outputs from the discriminator was fed to a channel of the time-to-digital-converter (TDC) module (LRS 226A) for measuring the arrival time of the signal in the detector. The pulses from the discriminators for T_{1E} and T_{1W} were also fed to a passive fan-in whose output pulse goes to the coincidence module for event selection. The other input to the coincidence module was the CAL pulse which was generated by discriminating the pulse obtained from a linear sum of pulses from the dynodes of photomultipliers viewing the 14 scintillator tanks in the calorimeter. While a single particle was sufficient to trigger the T_1 discriminators, the CAL pulse required about 50 GeV energy deposit in the calorimeter. The coincidence ($T_1\cdot$CAL) generated the master trigger which provided the gates to all the ADC modules and started the data read cycle. The anode pulses from the photomultipliers for the scintillator tanks in the calorimeter were connected directly to the ADC modules (LRS 2248) which were gated by the master trigger. The anode pulse from T_3 (and separately T_5) was fed after passive splitting to a discriminator and to a channel of the SHA-ADC system. One of the output pulses from the discriminator was fed to a channel of the TDC module. For the detector T_3 the other output pulse from the discriminator was used to generate the START gate to the TDC module in coincidence with the master trigger generated by the coincidence ($T_1\cdot$CAL). The anode pulses from the photomultipliers for the shower counters D_1 and D_2 were fed directly to the SHA-ADC system. The triggering threshold for the discriminator for T_3 was set at 3 particles and for T_5 at 30 particles The readout cycle initiated by the ($T_1\cdot$CAL) coin-

TABLE I. Details of run time and event-selection conditions for different runs.

Run No.	Period	Effective run time (h)	Effective T_1 (particles)	Selection CAL (GeV)	Threshold T_3 (particles)	Threshold D_1, D_2 (particles)
I(a)	April–July 1975	1072	1	50	25	1
I(b)	January–May 1976	1283				
II	July 1975–January 1976	3750	1	50	3	9

cidence pulse transferred data from the ADC's TDC, event counter, and clock modules to the magnetic tape through the Magtape Interface module.

All the detectors were calibrated routinely using near-vertical relativistic muons. Also, all the ADC and TDC modules were calibrated frequently to maintain a check on the conversion factors from charge and time intervals to digitized outputs.

Since the present experiment was only one of the several experiments[13–16] being carried out using basically the same detector system, a loose trigger was used to select events and various other cuts on data were imposed during analysis. Basically all events which had one or more particles in T_1 and more than 50 GeV energy release in calorimeter were selected by the (T_1·CAL) coincidence and recorded. However, the discriminator threshold for the detector T_3 was changed during the experiment to study hadrons of different threshold energies. Similarly gains for the photomultipliers for the shower counter were also changed during the course of the experiment. Basically there were three separate runs with somewhat different selection thresholds for the detectors T_3, D_1, and D_2. The details for these runs are given in Table I which gives the effective thresholds for various detectors.

C. Data analysis

The digitized outputs for various detectors for each event recorded on magtape were converted to an equivalent number of particles using the muon calibrations. Basically there are four quantities of interest for each event in this experiment: (i) the shower density near the detected hadron as given by the shower counters, (ii) the energy of the hadron detected by T_3 in terms of an equivalent number of particles traversing T_3, (iii) the hadronic energy (total) in the calorimeter obtained by summing the number of particles measured in all 14 scintillator tanks of the calorimeter and converting this particle sum to energy using the conversion factor given by Monte Carlo simulation[17] of hadronic cascades in this calorimeter, and (iv) the arrival-time delay of the signal in T_3 in nanoseconds relative to the mean of the arrival times of shower particles in T_{1E} and T_{1W}.

As mentioned earlier, an additional plastic scintillation detector T_5, of the same area as T_3, was placed above T_3 in 1975 and the amplitude and the arrival time of the signal from this detector was also digitized and recorded. However, since the threshold for the discriminator for T_5 was kept at 30 particles in order to study specifically the very-high-energy hadrons, the information from T_5 is not very useful in a discussion of the bulk of low-energy delayed hadrons.

D. Energy and timing resolution

The conversion of observed signals from various detectors in the calorimeter to energy has been studied both theoretically[17,18] and experimentally[19,20] and estimates for the accuracy of energy measurement have been obtained from these studies. The energy resolution for our calorimeter has been estimated from Monte Carlo simulations[17] which have predicted results in good agreement with accelerator calibrations[20] of other calorimeters. The expected resolution is about 25% for single hadrons of energies larger than 50 GeV and it improves with increasing energy. However, in studies of hadron component of air showers, multiple hadrons[21] are incident on the calorimeter resulting in an improvement in resolution for the measurement of total energy incident on the calorimeter. Most of the delayed hadrons are of low energy ($\sim 5-20$ GeV) and therefore, these resolution figures do not apply for the estimate of energy for these hadrons. The energy of these hadrons has to be estimated basically from the single measurement of the pulse amplitude observed in the detector T_3. Large fluctuations could be ex-

pected in the pulse amplitude for the same energy for several reasons: (i) the interaction point for the hadron is unknown, (ii) there are fluctuations in the development of the cascade, and (iii) there are fluctuations in the pulse amplitude due to large deposit of ionization in the detector by particles traveling at large angles and by slow heavily ionizing particles in the cascade. Since these fluctuations cause large uncertainties in the estimates for the energy of the hadrons, no attempt has been made to assign energy to the observed hadrons on an individual basis. However, these fluctuations have been taken into consideration in the Monte Carlo simulations of the hadron cascades in the calorimeter in a simple way. These are discussed in detail in Sec. IV.

The timing resolution has been estimated from a study of the distribution of the difference in arrival times as measured by the detectors T_{1E} and T_{1W} for dense showers. This distribution is shown in Fig. 3 for run I where the shower detectors D_1 and D_2 required a minimum particle density of 2 m^{-2}. For most of the events plotted in Fig. 3 the number of particles traversing each of T_{1E} and T_{1W} would be larger than eight. This distribution is nearly Gaussian with a standard deviation $\sigma \sim 3.5$ nsec. Since both the detectors T_{1E} and T_{1W} are very similar to each other and flucuations in them are nearly independent, the time resolution for each of these detectors can be taken as $3.5/\sqrt{2} \sim 2.5$ nsec. It may be noted that time slewing due to finite rise time (~ 5 nsec) of the pulses from T_1's does not have any effect on the distribution shown in Fig. 3 since the discriminator threshold for T_1's is only about 0.2 particle. Also, since the average zenith angle of showers is expected to be about 25° with practically no showers arriving at angles larger than 45° due to steep angular distribution

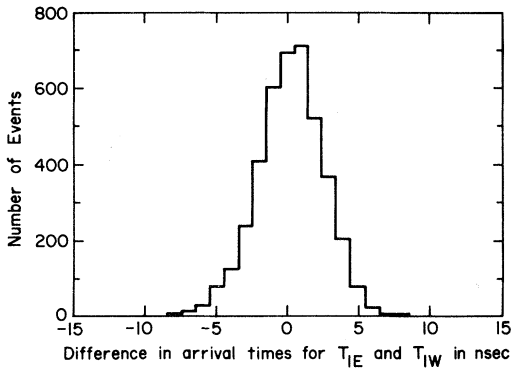

FIG. 3. Distribution of the difference in arrival time measured by shower counters T_{1E} and T_{1W} for dense showers.

($\sim \cos^7\theta \, d\theta$) and since the separation between the centers of these two detectors is only 0.9 m, the effect of angle of showers on σ is expected to be negligible. Since the electronics for the detector T_3 are also very similar to that for T_1's the effective time resolution for T_3 is also 2.5 nsec.

III. EXPERIMENTAL RESULTS

Since events were selected in the experiment with a general trigger additional selection conditions have been imposed on the data during analysis to select showers with some well-defined parameters. This was necessary to facilitate a comparison of the experimental results with expectations from Monte Carlo—simulated showers with the similar parameters. These conditions are as follows. (i) Each of the detectors T_{1E} and T_{1W} have more than eight particles, (ii) each of the detectors D_1 and D_2 have triggered (threshold of one particle in run I and nine particles in run II), (iii) total energy deposit in the calorimeter more than 50 GeV, (iv) the arrival times of shower electrons measured by T_{1E} and T_{1W} agree to within ~ 5 nsec, and (v) the number of particles in T_3 is above threshold for the timing discriminator (25 particles in run I and 3 particles in run II).

The delay distributions for the signal in T_3 were obtained for the events which met these selection conditions. Since the arrival delay of the hadron triggering T_3 is sensitively related to the energy of the hadron and therefore to the amplitude of the signal in T_3, the experimental data are best presented in terms of plots of the pulse amplitude in T_3 versus the delay measured by T_3 relative to the average arrival time of the shower front over T_1's. Such a plot for the events collected in run I is shown in Fig. 4(a). A similar plot for events observed in run II is shown in Fig. 4(b).

Figure 4(a) shows that there are three events which have rather large (~ 50 particles) deposits of energy in detector T_3 delayed by more than 30 nsec relative to the shower front. These delayed energetic events have been discussed in detail elsewhere.[12] Because of the high threshold for T_3 no low-pulse-amplitude delayed events were recorded in run I. Therefore, events observed during run I would not be discussed any further in this paper. However, the observed event rate during run I with selection conditions mentioned above is an important piece of information and will be used later for comparison with the rate expected from Monte Carlo simulation.

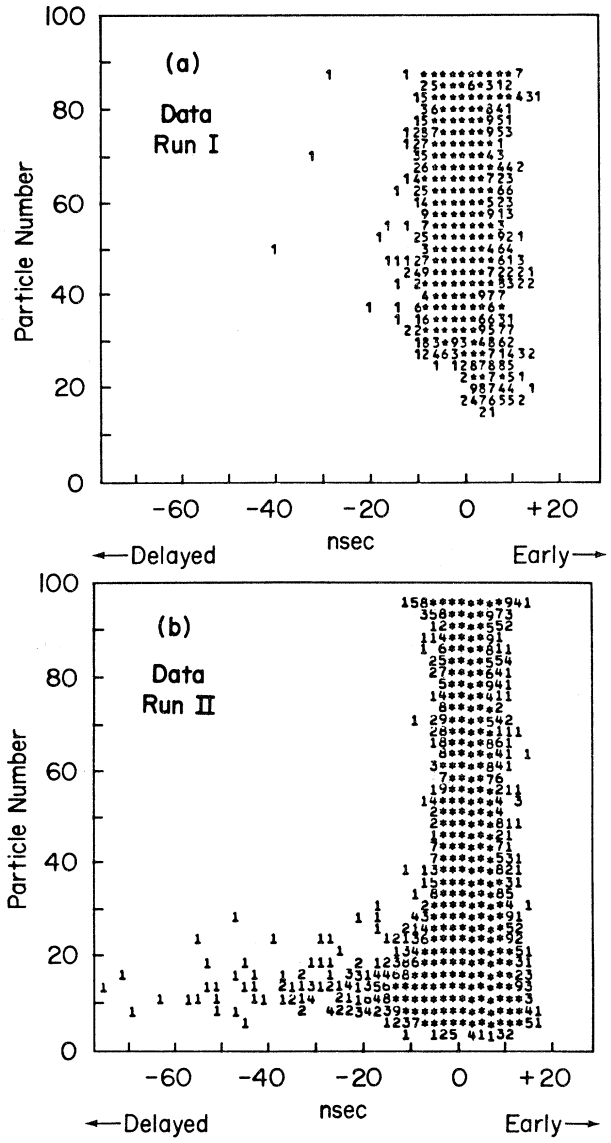

FIG. 4. A plot of the pulse amplitude in T_3 versus its arrival-time delay relative to shower detectors for events collected in (a) run I, and (b) run II.

Figure 4(b) shows the existence of a significant number of delayed low-energy hadrons which have given $\sim 5-20$-particle signal in T_3 and have delays extending beyond 100 nsec. The number of events with delays larger than 15 nsec and pulse amplitude in T_3 larger than five equivalent particles is 118. These delayed events constitute $(0.55\pm 0.05)\%$ of all events observed in run II which have shown signals larger than five particles in T_3 [Fig. 4(b)]. Similar delayed events have been observed in earlier experiments[22,23] and have been interpreted[24] as nucleons produced in high-energy hadronic interactions occurring in the cores of air showers. However, earlier experiments have studied delayed events with very different selection conditions which did not enhance the sensitivity of the experimental results to the composition of primary cosmic rays. In the present experiment such an enhancement has been achieved by requiring a large amount of hadronic energy near the delayed hadron as discussed in detail in Sec. V. For comparing the delay distributions for hadrons of different energies, projections of the data shown in Fig. 4(b) on the delay axis for different regions of pulse amplitudes in T_3 (5—15, 15—30, 30—45, and >45 particles) are shown in Fig. 5. The plots in Fig. 5 show that low-energy delayed hadrons are almost all in the 5—30-particle range for T_3 signal and the delayed energetic events shown in Fig. 4(a) are distinct from the delayed events shown in Fig. 4(b). A sharp cutoff on the "early" side is clearly seen indicating the absence of accidental coincidences.

The experimental results are summarized for later comparison with expectation from Monte Carlo simulation of observations with selection conditions as specified earlier in this section, as follows.

(i) The observed rate of selected events in run I is $9135/(7.65\times 10^6\ \mathrm{m^2 sr\,sec}) = 1.19\times 10^{-3}\ \mathrm{m^{-2} sr\,sec^{-1}}$.

(ii) The observed rate of selected events in run II is $21\,480/(1.16\times 10^7\ \mathrm{m^2 sr\,sec}) = 1.85\times 10^{-3}\ \mathrm{m^{-2} sr^{-1} sec^{-1}}$.

(iii) The fraction of events with delays larger than 15 nsec among all events with signal larger than five particles selected in run II is $(0.55\pm 0.05)\%$.

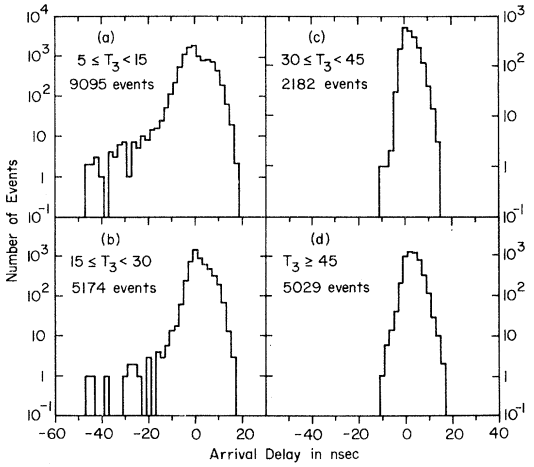

FIG. 5. Distributions of arrival-time delay for different amplitudes of the signal from the hadron detector T_3 (run II).

IV. MONTE CARLO SIMULATION

Hadrons observed at mountain level or sea level are the product of a large number of interactions occurring at various altitudes in the atmosphere. Therefore, it is necessary to simulate in detail the development of air showers for a meaningful comparison with the experimental results. Basically there are three components in this simulation which need to be specified: (i) flux and energy spectra for various nuclei in primary cosmic rays in order to choose the type and energy of the proginator of individual air showers, (ii) interaction model and details of propagation of the hadron-electron-photon cascade in the atmosphere up to the observational level, and (iii) experimental selection conditions and instrumental response functions.

The primary aim of this study is to find the relative fractions of various nuclear groups in primary cosmic rays and the variation of this composition with energy, hence energy spectra of various nuclear groups are not specified *a priori*. The method adopted here to achieve this objective is to find out the efficiency factor ϵ for generating an "observed" event for different primary energies and different primary nuclei by simulating air showers and instrumental responses for each of these combinations. Using these efficiency factors we match the observed frequency of events with various combinations of relative composition and energy spectra for different nuclear groups. The observed delayed fraction is then used to limit these possibilities and obtain a consistent and plausible answer for the composition of primary cosmic rays and its variation with energy.

A. Interaction model and the hadron cascade

Hadronic interactions have been simulated with an independent particle emission model. Secondary momenta in the center of mass (c.m.) are drawn at random from probability distributions obtained from Feynman[6] scaling of the invariant single-particle inclusive cross sections. Secondary particles are created until the available c.m. energy is exhausted. No correlations between longitudinal and transverse secondary momenta have been assumed. The effects due to the nuclear composition of the target have been neglected here and the target has been assumed to be a nucleon in all interactions. Since shower development is dominated by energetic forward secondaries and the present study is confined to near-core regions due to the requirement of 50 GeV in the calorimeter, the increase in multiplicity observed[25] for hadron-nuclear interactions is not expected to produce a significant effect on results. Showers initiated by primary nuclei were simulated using superposition assumption. Thus the shower initiated by a nucleus of atomic number A and energy E_0 is taken to be the sum of A showers due to A nucleons, each of energy E_0/A, interacting independently. The details of various other assumptions and the simulation procedure are as follows.

(i) Since the observed showers were selected independent of their angles relative to zenith, the zenith angle for the primaries of simulated showers have been picked randomly from a $\cos\theta$ distribution.

(ii) The inelastic cross sections[26] for hadron-air nucleus collisions have been assumed to be energy dependent and the parametrization used is

$$\sigma_{p\text{-air}}^{\text{inel}}=[260+11\ln(E/100)]\ \text{mb}$$

(E in GeV) and

$$\sigma_{\pi-\text{air}}^{\text{inel}},\sigma_{K-\text{air}}^{\text{inel}}=0.72\sigma_{p-\text{air}}^{\text{inel}}\ .$$

(iii) The c.m. longitudinal momenta of the incident particle and the target nucleon after the interaction are chosen independently. For incident protons the x ($=2p_l^*/\sqrt{s}$, p_l^* is the c.m. longitudinal momentum and $\sqrt{s}$ is the available c.m. energy) distribution is assumed to be flat, i.e., $dn/dx=$constant, in rough agreement[4] with accelerator data on leading particles in p-p collisions. This assumption yields a mean inelasticity of 0.5. Available data[27] on π-p collisions was approximated to a steplike distribution for picking x for leading pions and kaons yielding a value of 0.72 for mean inelasticity.

(iv) The c.m. longitudinal momenta of secondary particles (pions, kaons, and nucleons) are picked from the x distributions corresponding to the form

$$E\frac{d^3\sigma}{dp^3}\propto e^{-Ax}$$

for the invariant inclusive cross sections. The value of A has been chosen to be either 4.5 or 5.5 (with equal probability in individual interactions) in nucleon-nucleon collisions. For pion-nucleon and kaon-nucleon collisions the corresponding values of A are 2.5 and 3.4.

Each secondary particle is assigned to be a nucleon (or antinucleon), kaon, or pion through a random selection based on assumed relative pro-

duction probabilities. Since delayed hadrons in air showers have been shown[24] to be mostly nucleons, it is clear that baryon production at higher energies plays a significant role for interpretation of data on arrival-time distribution for hadrons in air showers. Based upon CERN ISR observations[28] and extensive-air-shower experiments[24] nucleon-antinucleon production has been assumed to be energy dependent and the probability f_N for a produced particle to be a nucleon (proton, neutron, antiproton, or antineutron with equal probability) has been taken as

$$f_N = 0.0164 \ln(1 + 0.015 E_{\text{lab}}) ,$$

where E_{lab} is the energy in GeV of the incident particle in the laboratory system. This parametrization is in good agreement with accelerator data[28] on $\bar{p}$ production at ISR energy. The value of the parameter A for secondary nucleons has been taken as 11.0 to account for their steeper x distributions. The probability for a secondary particle to be a kaon has been assumed to be 0.10 and energy independent. A particle not assigned to be a nucleon or a kaon is assumed to be a pion. Pions are randomly tagged as neutral with an average probability of 0.33.

The assumed shape of the x distribution for various particles plays a dominant role in the development of air showers in the atmosphere. The invariant cross sections assumed in simulations are compared with available experimental data[29] on p-p and π-p collisions in Fig. 6. This comparison shows that the assumptions underlying the simulations give a good representation of the experimental data at ISR energies.

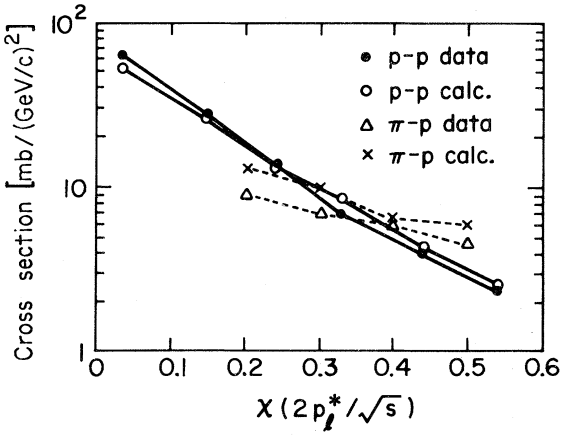

FIG. 6. A comparison of the x distribution for charged pions produced in p-p and π-p collisions assumed in Monte Carlo simulations with data from ISR experiments (Ref. 29).

(v) The transverse momenta of all particles are chosen from an exponential-type transverse-momentum distribution

$$\frac{dn}{dp_t} \sim A p_t e^{-Bp_t}$$

with the value of B assumed to be 6 $(\text{GeV}/c)^{-1}$ for pions and kaons and 4 $(\text{GeV}/c)^{-1}$ for nucleons. However, the exponential distribution is known[30] to be valid only for small ($\lesssim 1-2$ GeV/c) values of p_t. The form of the large-p_t component has been taken from the work of Halzen and Luthe[31] which also gives parametrization of the energy dependence for the large-p_t component. The distribution

$$\frac{dn}{dp_t} \propto p_t/(p_t^2+1)^2$$

was used to pick the value of p_t with a probability of $3.36\times 10^{-4} s^{0.6}$ (s in GeV^2).

The azimuthal angles for the secondary particles are chosen at random and approximate momentum conservation is obtained by pointing the c.m. momentum vector into the hemisphere opposite to that of the sum of all previous momenta in the interaction.

(vi) After the momentum of each particle is determined the total amount of c.m. energy used so far is computed. If the most recently created particle makes the total energy greater than the actual c.m. energy, this particle is randomly included 50% of the time, and the momenta are Lorentz transformed to the laboratory system. If there is more energy available, more secondaries are produced until the available energy is used up. The lack of exact energy conservation is, on the average, at a level of only about 4% in this procedure because most of the produced particles are of low energy.

(vii) The time delay for each hadron is computed relative to a particle of velocity c moving along the shower axis and the accumulated delay for each hadron is stored.

(viii) The spatial coordinates and the momenta of each neutral pion are also stored for simulation of shower density as discussed later.

All the hadrons produced in various interactions are followed through the atmosphere until either they reach the observational level or their energy becomes less than 3 GeV. Backward-going particles in the laboratory system are rejected. Charged pions and kaons are allowed to decay with appropriate probabilities. The coordinates, the type, and the energy of each hadron reaching the obser-

vational level are recorded. Some information about the last interaction which produced the particle is also stored. For example, it is known for each particle whether it is a surviving primary, a target nucleon, or a created particle.

An approximation to the standard atmosphere is used in the simulation. This fit uses two functions, one for depths up to 220 g cm^{-2} from top of the atmosphere and the other for lower atmosphere. Therefore, the height above sea level, h in kilometers, is related to the pressure x (g cm^{-2}) as

$$h = 45.45 - 6.335[\ln(x)] \text{ for } x \leq 220 \text{ g cm}^{-2}$$

and

$$h = 44.342 - 11.865(x)^{0.19} \text{ for } x > 220 \text{ g cm}^{-2} .$$

Since the selection conditions in the experiment required a shower particle density of 18 m^{-2} (run II) near the hadron detected in the calorimeter, shower density is calculated for the coordinates of each hadron generated by the hadron cascade which has reached the observational level. For this purpose each stored π^0 is decayed into two γ rays and the contribution of each γ ray to the shower density is calculated. Approximation B (Ref. 32) has been used to compute the shower age as well as the total number of electrons at the observational level. The modified Nishimura-Kamata-Greisen (NKG) lateral distribution function proposed by Hillas and Lapikens[33] has been used to compute the shower density at the coordinates of each hadron.

The position, type, energy, time delay, and the local electron density for each hadron is therefore known.

B. Simulation of instrumental response

The experimental requirements of a deposit of 50 GeV or more in the calorimeter and a signal above the threshold level in T_3 was put on the Monte Carlo–simulated (MCS) hadrons. However, since the upper detector layer of the calorimeter also responds to the remnants of energetic electron-photon cascades, it was estimated that the minimum hadronic energy required in the calorimeter was only 30 GeV. Therefore for each MCS hadron, assumed to be incident on a fictitious detector T_3, the energies of all hadrons incident on the surrounding area of 4 m^2 were summed. The MCS hadron was selected for further consideration only if this sum was larger than 30 GeV.

In the experiment, events with two or more hadrons over T_3 are not distinguished from events with only one hadron incident over T_3 and the arrival time of the earliest of these hadrons, which gives enough signal to trigger the timing discriminator, is measured. In simulations the contributions of the signal in T_3 due to various hadrons incident over the area of the fictitious detector are summed, and the arrival time of the earliest hadron is taken as the arrival time of the simulated event. The time of arrival of each MCS hadron is picked from a Gaussian curve with σ of 3 nsec around the computed time (all relative to shower front) to simulate the fluctuation in measurement of arrival time.

The cascade of the hadron whose arrival time is measured in the experiment is sampled only by detector T_3 located at a depth of 220 g cm^{-2} (iron) in the calorimeter, therefore it is necessary to simulate this feature in the calculations. For this purpose, the distributions of equivalent number of particles in a detector like T_3 for hadrons of various energies for this calorimeter have been used. These were obtained from Monte Carlo calculations by Jones[17] for our calorimeter. For each MCS hadron incident over the fictitious T_3, an equivalent particle number is obtained through a random process from the distribution corresponding to its energy. It may be noted that this distribution takes care of cascades that are absorbed before reaching T_3 and also cascades which have not started before T_3 due to fluctuations in the point of first interaction. A sum is taken for the equivalent number of particles obtained for various hadrons incident over T_3 in the same event. The distribution of equivalent number of particles in T_3

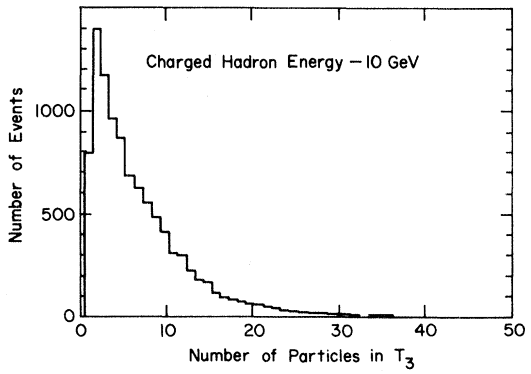

FIG. 7. Distribution of the expected signal from T_3 for nucleons of energy 10 GeV incident on the calorimeter.

for vertically incident hadrons of energy of 10 GeV, given by the calculations of Jones,[17] is shown in Fig. 7. Experimental data for a similar type of detectors by Whiteside *et al.*[34] have shown a factor of 1.2 in the number of particles relative to calculations by Jones and as a factor of ~ 1.2 is expected for inclined cascades, the numbers shown in Fig. 7 have been multiplied by 1.4 for computing the expected signal in T_3.

V. RESULTS FROM SIMULATIONS AND COMPARISON WITH EXPERIMENTAL DATA

Each MCS hadron which satisfies the experimental selection conditions, as discussed in the last section, is potentially detectable as an individual event in the experiment. The number of such hadrons in an air shower can be considered as the efficiency for generating observable events by the primary particle initiating the shower. This efficiency factor, called $\epsilon(E,A)$ here, depends on the energy per nucleon E and the atomic number A of the primary nuclei. It has been computed from simulations for various values of E and A. The dependence of ϵ on E for showers initiated by various nuclei is shown in Fig. 8 for hadrons selected with selection conditions corresponding to run II. It is seen that the efficiency increases with primary energy and is higher for proton-initiated showers relative to iron-nucleus-initiated showers for the same total energy. However, it is interesting to note that the efficiency factor does not continue to increase monotonically. This behavior is a result of the imposition of a shower-density requirement. At lower energies only hadrons very near the core are accompanied by a shower of sufficiently high density to satisfy the selection conditions. As the primary energy increases the region with shower density above threshold widens and also the number of hadrons arriving at the observational level increases. Therefore, the number of acceptable hadrons increase rapidly with primary energy. For sufficiently high energies most of the hadrons with energy above the energy threshold of the calorimeter are accompanied by shower density well above the selection threshold. However, many of these hadrons are incident over the detector in the same shower. Thus the rate of growth of the efficiency curve slows down reflecting only the increase in the number of separately resolvable hadrons above threshold energy.

It is of interest to study the arrival-time distribu-

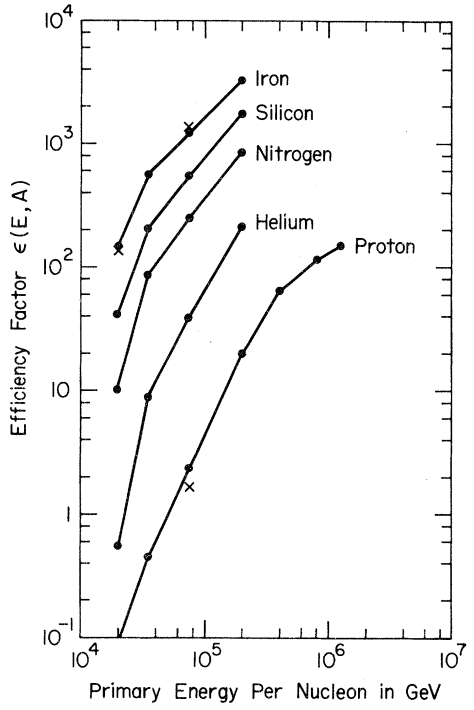

FIG. 8. Variation of the efficiency factor $\epsilon(E,A)$ defined as the number of observable hadrons satisfying the selection conditions of run II of the experiment per shower, with primary energy for different primary nuclei (x, modified scaling model).

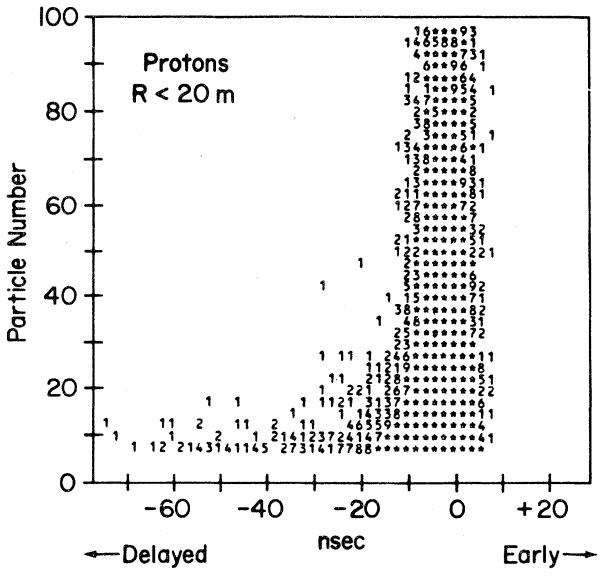

FIG. 9. A plot of the expected pulse amplitude in T_3 versus its expected arrival-time delay relative to the shower front for hadrons located within 20 m of the core of showers initiated by proton primaries.

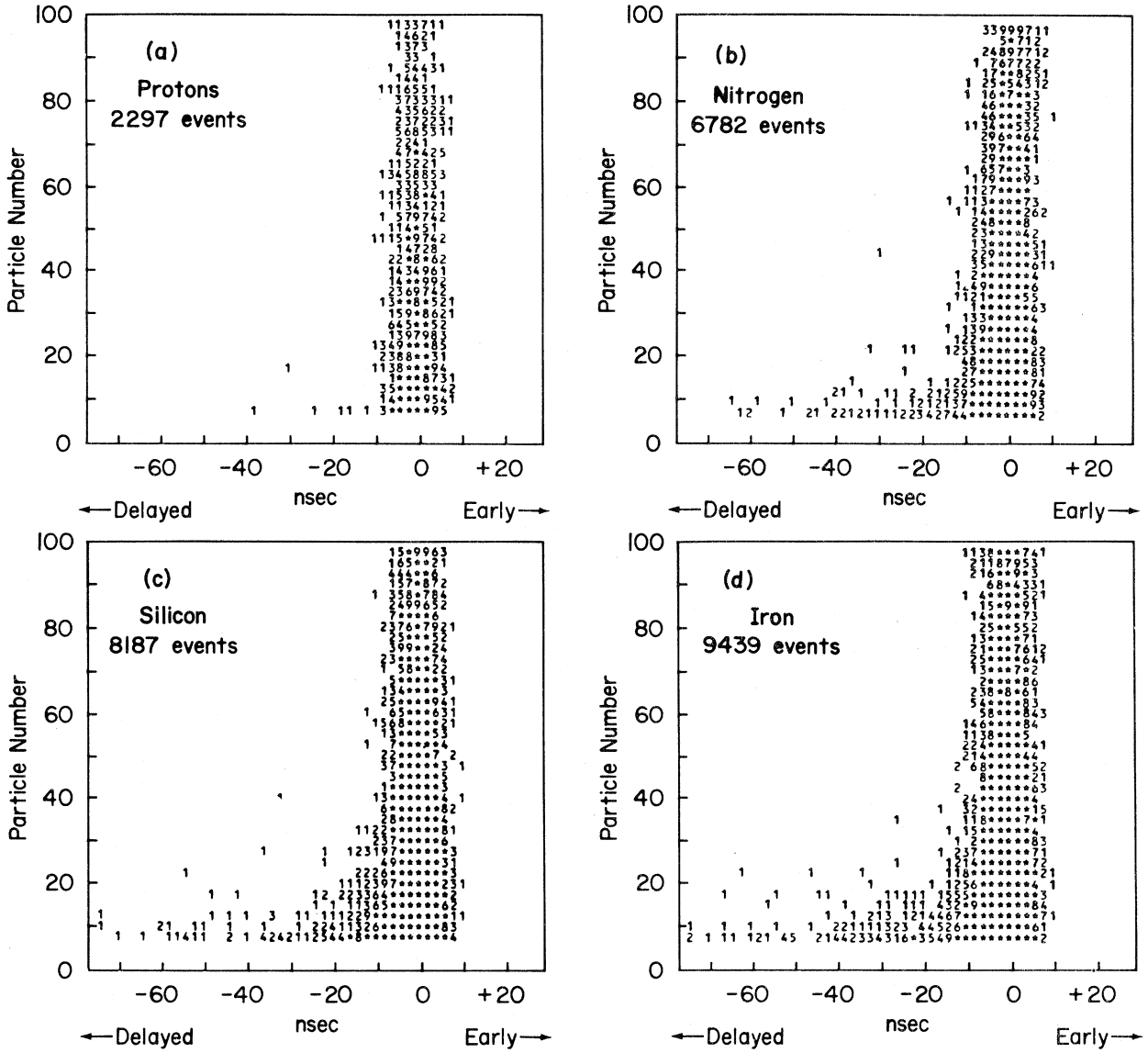

FIG. 10. A plot of the expected pulse amplitude in T_3 versus its expected arrival-time delay relative to the shower front for hadrons satisfying the selection conditions of run II in showers initiated by (a) protons, (b) nitrogen nuclei, (c) silicon nuclei, and (d) iron nuclei.

tion of hadrons in simulated showers, initially, without imposing the selection conditions of the present experiment. The plot of the hadron energy versus the arrival delay of hadrons located within 20 m of the shower core for proton-initiated showers is shown in Fig. 9. The hadron energy is expressed here as the signal in equivalent number of particles expected from T_3. The energies of primary protons were picked from a differential energy spectrum $dN \propto E^{-2.7}dE$ for E larger than 10 TeV. It is seen that with this selection condition proton showers do give delayed hadrons. Consequently showers initiated by heavy nuclei can also be expected to produce similar distribution of delayed hadrons since they are taken to be a superposition of proton showers. Experiments which only require that hadrons be within a fixed distance from the shower core would thus observe delayed hadrons from both proton- and heavy-nucleus-initiated showers. Distributions similar to those shown in Fig. 9 have been observed in Ooty experiments by Tonwar *et al.*[24] However, as pointed out by Tonwar and Viswanath,[35] Ooty experiments are not sensitive to heavy-nuclei showers due to the requirement of constant shower size since proton showers are preferentially selected in showers

grouped according to shower size.

The imposition of experimental selection conditions corresponding to run II on the results from Monte Carlo simulations yields a significantly different delay distribution. The plots of expected signal from T_3 versus time delay for hadrons in showers initiated by proton, nitrogen, silicon, and iron nuclei are shown in Figs. 10(a), 10(b), 10(c), and 10(d), respectively, for selection conditions of run II. It is seen that very few hadrons, delayed by more than 10 nsec, pass the selection conditions for proton showers. However, a significantly larger number of delayed hadrons satisfy the selection conditions in showers initiated by heavy nuclei. A comparison of these four figures [10(a)—10(d)] clearly shows the sensitivity of the arrival-time distribution of hadrons to primary composition due to the selection conditions imposed in the collection of data in run II of the present experiment. The variation of the fractional number of hadrons delayed by more than 15 nsec among those which give a signal larger than five equivalent particles in T_3 with the mass number of primary nucleus initiating the shower is shown in Fig. 11.

Qualitatively this high sensitivity of the time distribution to primary composition can be understood in terms of flatter lateral distribution[21,36] of hadrons as well as of electrons for iron-nucleus-initiated showers compared to proton showers.

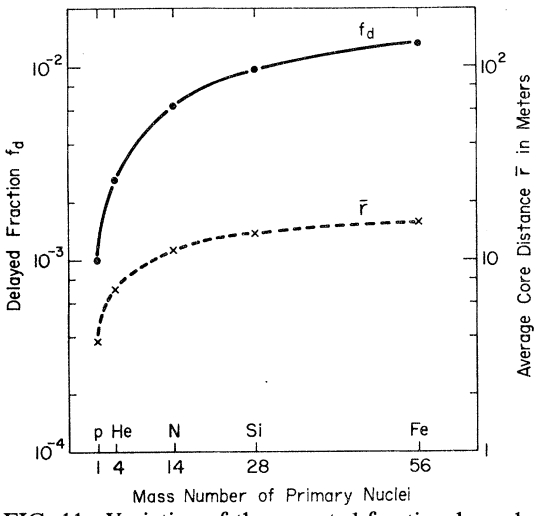

FIG. 11. Variation of the expected fractional number of hadrons, satisfying selection conditions of run II, delayed by 15 nsec or more with mass number of the primary nucleus initiating the shower. Also shown is the variation of the average core distance of these hadrons (prompt and delayed) with mass number.

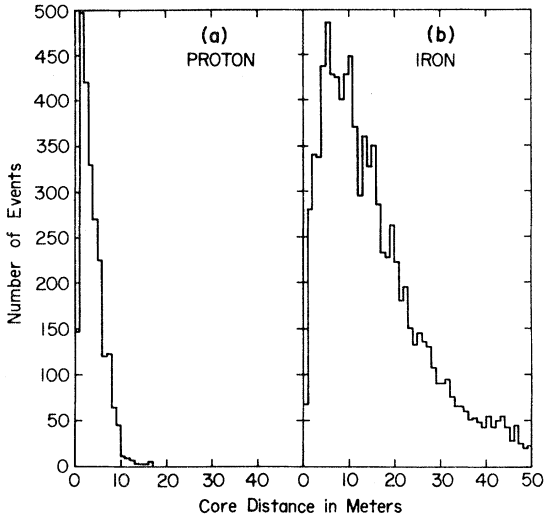

FIG. 12. Expected lateral distribution of hadrons satisfying the selection conditions of run II in showers initiated by (a) protons and (b) iron nuclei.

Low-energy hadrons arrive delayed when they travel substantial distances from their production points. Since the transverse momentum is independent of energy, these hadrons tend to be laterally displaced farther from the core than the energetic nondelayed hadrons. However, the energy of these particles is insufficient to provide the energy requirement for the calorimeter trigger. Only in heavy-nuclei-initiated showers are there sufficient numbers of other hadrons at these distances to satisfy the energy selection criterion. Similarly, the shower density required to generate a trigger at these larger distances is also available in older showers preferentially due to their flatter electron lateral distribution. The average distance of hadrons satisfying the selection conditions of run II for showers initiated by various nuclei is shown in Fig. 11 as a function of the mass number of primary nucleus. (See also Fig. 12.) It is seen that hadrons are selected up to much larger distances from the shower core for showers initiated by heavy nuclei, which results in larger collection areas for these showers. Another reason for the high sensitivity for primary composition in the present experiment is the nature of delayed hadrons which are mostly nucleons. The number of interactions which produce secondary nucleons and also recoil nucleons is much larger in showers initiated by heavy nuclei as compared to showers initiated by protons and lighter nuclei.

Since the efficiencies for generating an observable event have been obtained from simulations for selection conditions of run I as well as of run II, it

is relatively straightforward to determine the expected rate of events for comparison with observations. The expected number n_d of detectable hadrons per unit time is

$$n_d = (\text{area}-\text{solid-angle factor}) \times \sum_A \int_0^\infty \frac{dn(A)}{dE}\epsilon(A,E)dE \ , \quad (5.1)$$

where $dn(A)/dE$ is the differential energy spectrum of primary nuclei of mass number A. The solid-angle—area factor cannot be estimated in a direct manner for the present experiment because arrival angles of detected showers were not measured experimentally. However, this fact has been taken into consideration in the simulations where showers have been generated from an isotropic flux at the top of the atmosphere. Calculations have shown that very few showers arriving with zenith angles larger than 45° provide a detectable hadron, mainly due to the much larger primary energy required to give hadron energy and shower density.

Therefore, a cut of 45° was put on the zenith angle of simulated showers and the solid-angle—area factor has been taken to be $\pi D/2$ corresponding to isotropic angular distributions where D is the area of T_3. Note that the effects expected due to observed steep angular distribution of showers at mountain altitude ($\sim\cos^n\theta$, $n\sim 7-8$) are included in the determination of the efficiency factor $\epsilon(A,E)$.

The summation in the relation (5.1) is over all species of nuclei present in the primary flux. Since there are no direct measurements available for the energy spectra of primary cosmic rays above energies of a few hundred GeV per nucleon, it is necessary to make some plausible assumptions about the shape of the spectra for various nuclei, guided by the currently popular ideas[37] on cosmic-ray origin and propagation in interstellar space. The free parameters available in these assumed models of primary composition and its variation with energy, for example, the exponents of the power-law spectra, can then be determined from a comparison of the expected event rate with the observed rate for both runs I and II. Two possible models[38] for primary energy spectra and compositions are considered.

(i) Model I. In this simple model the energy spectra of protons, α particles, light nuclei (CNO group), and medium-heavy nuclei (MH group, $10<Z\leq 16$) are assumed to be power-law type with the same exponent γ_L which itself is treated as a free parameter,

TABLE II. Values of energy and flux used for normalization of spectra for various nuclei in different models.

Average mass number $\langle A\rangle$	Normalization energy (GeV/A)	E_0 (GeV/nucleus)	Differential flux (dn/dE) at $E=E_0$ [$m^{-2}sr^{-1}sec^{-1}(GeV/A)^{-1}$]
1	2000	2000	1.5×10^{-5}
4	300	1200	8.0×10^{-5}
14	250	3750	1.2×10^{-5}
28	75	1950	1.7×10^{-4}
56	63	3528	9.0×10^{-5}

$$dN_i = K_i E^{-\gamma_L} dE \ \text{m}^{-2}\text{sr}^{-1}\text{sec}^{-1}(\text{GeV}/A)^{-1} \ ,$$

where i represents proton, α, CNO, or MH nucleus, and here and subsequently E is in (GeV/A). Similarly the energy spectra of heavy nuclei (H group, $26\leq Z<30$) are also assumed to be power-law type, however, with a different exponent γ_H, also treated as a free parameter,

$$dN_H = K_H E^{-\gamma_H} dE \ \text{m}^{-2}\text{sr}^{-1}\text{sec}^{-1}(\text{GeV}/A)^{-1} \ .$$

For simplicity the CNO, MH, and H nuclei groups have been assumed to have the average atomic numbers of 14, 28, and 56, respectively. The constants K_i's and K_H have been determined by normalization to direct measurements[2] of energy spectra at lower energies. Table II gives the normalization energy and flux for nuclei of various groups which have been used to compute the values of K's in the different models discussed here. For example, the values of K for a value of -2.71 for γ_L

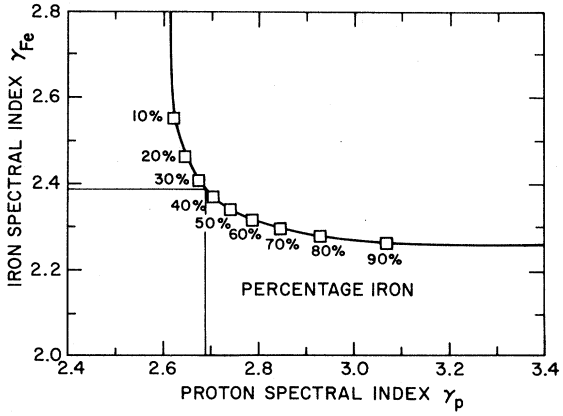

FIG. 13. A plot of the relation between the value of γ_p, the power-law spectral index for protons and lighter nuclei and γ_{Fe}, the spectral index for iron-group nuclei, necessary for obtaining a good agreement of the expected event rate with the observed rate for hadrons detected in run II.

are 13 240, 413, 38, and 20 for proton, He, N, and Si nuclei, respectively. The value of K for H nuclei for a value of -2.36 for γ_H is 1.6. The expected event rate for discrete values of primary energy E is just a product of the efficiency factor ϵ and the differential flux for energy E. Integration over energy gives the expected event rate due to different nuclei and the sum of these numbers then gives the expected event rate for the assumed values of γ_L and γ_H which can be compared to the observed rate. Since any change made in γ_L necessitates a change in the assumed value of γ_H in order to keep the expected event rate unaltered and equal to the observed rate, the parameters γ_L and γ_H are related. Figure 13 shows the relationship expected between γ_L and γ_H for giving a good agreement between the expected event rate and observations for run II.

The information on event rate by itself is not sufficient to distinguish between various possible combinations of γ_L and γ_H represented by different points on a contour curve in Fig. 13. However, each point on this curve defines a relative composition of various nuclear groups and it is possible to calculate the expected delayed fraction for hadrons using the results given for different primary nuclei in Fig. 11. The variation of the expected delayed fraction for different values for the spectral exponents γ_L and γ_H is shown in Fig. 14(a) which also shows the expected event rate for these values. Since the observed delayed fraction for hadrons in run II is $(0.55\pm0.05)\%$ the only values of the spectral exponents that provide a simultaneous fit to the observed event rate and the observed delayed fraction are $\gamma_L=-2.68\pm0.06$ and $\gamma_H=-2.39\pm0.06$. Therefore, in model I the experimental results suggest the following forms for the energy spectra for various nuclear groups in primary flux:

$$dN_p = 10\,540\times E^{-2.68\pm0.06}\,\mathrm{m}^{-2}\mathrm{sr}^{-1}\mathrm{sec}^{-1}(\mathrm{GeV}/A)^{-1}$$

$$dN_\alpha = 348\times E^{-2.68}\,\mathrm{m}^{-2}\mathrm{sr}^{-1}\mathrm{sec}^{-1}(\mathrm{GeV}/A)^{-1}\,,$$

$$dN_{\mathrm{CNO}} = 32\times E^{-2.68}\,\mathrm{m}^{-2}\mathrm{sr}^{-1}\mathrm{sec}^{-1}(\mathrm{GeV}/A)^{-1}\,,$$

$$dN_{MH} = 18\times E^{-2.68}\,\mathrm{m}^{-2}\mathrm{sr}^{-1}\mathrm{sec}^{-1}(\mathrm{GeV}/A)^{-1}\,,$$

$$dN_H = 1.8\times E^{-2.39\pm0.06}\,\mathrm{m}^{-2}\mathrm{sr}^{-1}\mathrm{sec}^{-1}(\mathrm{GeV}/A)^{-1}\,.$$

It should be emphasized here that since the spectral exponent for He and MH nuclei has been assumed to be the same as for protons, the energy spectra for these nuclear groups have not been determined independently. However, their contributions to the expected event rate and also the delayed fraction have been taken into account using the spectra given above.

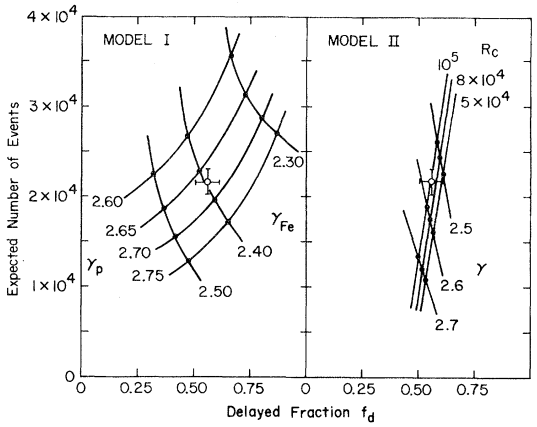

FIG. 14. Variation of the expected event rate with the delayed fraction for hadrons satisfying selection conditions of run II for various values of (a) the power-law spectral exponents γ_p and γ_{Fe} for protons (and lighter nuclei) and heavy nuclei, and (b) the power-law spectral exponent γ and the rigidity cutoff R_c (GV/c).

This analysis requires that the energy spectrum of iron-group nuclei is much flatter compared to the spectra for protons and lighter nuclei and that the heavy nuclei component becomes the dominant component at medium air-shower energies, 10^5-10^6 GeV. However, significant contributions to the observed hadron flux come from primary energy $\sim$100 TeV for protons and 1000 TeV for iron-group nuclei. A change in the energy spectra for heavy nuclei above energy of 1000 TeV would not cause any detectable change in the expected event rate. Therefore, from present results it is not possible to extend these energy spectra to much higher energies with same values of spectral exponents.

(ii) Model II. In this model it is assumed that the energy spectra of all nuclear groups have the same spectral exponent γ as at lower energies ($\leq 10^5$ GeV) but the spectra of different nuclear groups steepen above a critical rigidity value of R_c. The parameters γ and R_c are treated as free parameters. This model is inspired by the ideas of the nested leaky box model[39] for cosmic-ray propagation in the galaxy and it is assumed here that the spectrum of a given nuclear group becomes steeper by 0.5 above a critical rigidity. The value of R_c would be about a factor of 2 different for protons compared to the iron-group nuclei. Following the procedure described for model I, the expected event rate and the delayed fraction have been computed for various values of γ and R_c. These are shown

in Fig. 14(b). It is seen that a value of -2.55 for γ and 10^5 GV/c for R_c give a good agreement between the expected and observed quantities. The results obtained here also suggest that the heavy nuclei become a dominant component of primary cosmic-ray flux at energies $\sim 10^6$ GeV.

VI. DISCUSSION

The comparison of observed event rates and the delayed fraction of hadrons with the predictions from Monte Carlo simulation of air showers and the instrumental response in the previous section has clearly shown that a primary composition dominated by protons and light nuclei, similar to that at lower energies, cannot account for the observations. It is necessary to have either a flatter energy spectrum for the heavy-nuclei component at energies above ~ 100 GeV/A (model I) or a rigidity-dependent steepening of the energy spectra of protons and other nuclei above a critical rigidity $\sim 10^5$ GV/c (model II). In both of these models the iron-group nuclei become the dominant component in the primary flux at energies $\sim 10^5 - 10^6$ GeV, as shown in Fig. 15, reaching a value of about $40-60\,\%$ at 10^6 GeV. It may be remarked that the spectra and flux specified in both these models are consistent with the all-particle spectrum measured directly by Grigorov *et al.*[1] up to about 10^6 GeV. However, it is clear that the steepening[40] of the all-particle spectrum seen at $\sim 10^7$ GeV is not an integral part of the model I as assumed here. An additional mechanism would have to be introduced to account for the steepening. On the other hand, the steepening of the spectrum is an integral part of the model II. Further, in both models the assumption of the existence of an extragalactic component or a larger confinement region for the very-high-energy ($\geq 10^7$ GeV) cosmic rays is required to explain the dominance[40] of protons at energies $\sim 10^8 - 10^{10}$ GeV.

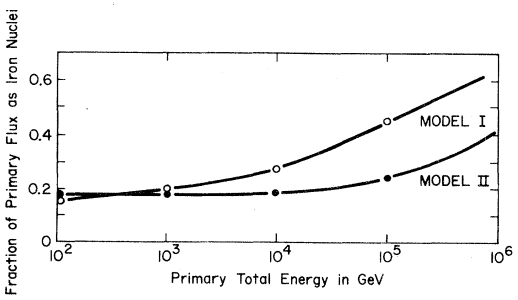

FIG. 15 Variation of the expected fractional content of heavy nuclei (iron group) in the primary cosmic-ray flux with primary energy for the two assumed models of primary energy spectra.

The presence of a significant proportion of heavy nuclei in primary flux at energies $\sim 10^5 - 10^7$ GeV has also been suggested by various other air-shower experiments. The data on multiple muons from underground experiments[41] have been shown[42] to require a composition rich in iron-group nuclei. Similarly the variation of the number of low-energy muons with shower size has been shown[43] to be inconsistent with the composition similar to that measured at low energies. Elbert *et al.*[42] have interpreted the data on the fluctuations in the number of muons as indicating the preponderance of iron nuclei in primary flux in the energy range $\sim 10^5 - 10^7$ GeV along with a smaller but non-negligible fraction of protons. Recently the studies on very-high-energy ($\gtrsim 100$ GeV) muons observed either in underground experiments[44,45] or with magnetic spectrometers[46] have also shown[21] that these observations cannot be understood in terms of proton-dominant composition at energies $\sim 10^5 - 10^6$ GeV. Many measurements[47] of the depth of shower maximum in the atmosphere using different techniques (study of size of showers with constant intensity for different zenith angles, study of the temporal profiles of Cerenkov light pulses, etc.) have also shown that the primary composition is changing with energy in the range $10^4 - 10^8$ GeV with heavy nuclei playing a dominant role at energies $\sim 10^5 - 10^7$ GeV. The results of these and other measurements in relation to the primary composition have been reviewed by Gaisser *et al.*[4] and more recently by Yodh.[5]

A. Sensitivity to particle-interaction model

Many of the air-shower results discussed above including the results on primary composition obtained in the present experiment have assumed validity of Feynman[6] scaling of single-particle inclusive cross sections with energy. However, Feynman[6] scaling has been shown to be mildly violated[48] even at ISR energies and a modified form, called radial scaling,[7] has been proposed to fit the accelerator data. For example, the observed rise in the height of the plateau in the rapidity distribution for particles produced in central region (Feynman variable $x \sim 0$) with energy, not expected for Feynman scaling, is reproduced well in radial scaling. Radial scaling has been used by various au-

thors[49,50] to interpret observations at higher energies. The basic question that arises in this context is the following: What is the form of the energy dependence of the average secondary-particle multiplicity at air-shower energies? It is of interest to know the extent to which the results on primary composition from the present experiment are affected by the energy dependence of multiplicity seen in experiments at ISR (Refs. 7, 49, and 50) and recently at the $\bar{p}p$ collider.[9] Since the energies of primary protons generating the observed events in the present experiments are, in general, lower than the equivalent laboratory energy ($\sim 1.5\times 10^5$ GeV) at the $\bar{p}p$ collider, extrapolation of interaction parameters to higher energies is not needed. The observed scaling violation has been simulated here by making the following changes in the assumptions discussed in Sec. IV.

The parameter A used in the x distribution

$$E\frac{d^3\sigma}{dp^3} \propto e^{-Ax}$$

for picking the c.m. longitudinal momenta of secondary particles has been assumed to increase with energy as

$$A = A_0 \text{ for } E < 1000 \text{ GeV} ,$$

$$A = A_0[1+\alpha \ln(E/1000)] \text{ for } E \geq 1000 \text{ GeV} ,$$

where the value of A_0 is the value assumed in the scaling model discussed in Sec. IV. The value of the parameter α as 0.33 has been determined from a fit of the expected average particle multiplicity to observed multiplicity at ISR energy and the estimated multiplicity at CERN SPS $\bar{p}p$-collider energy.

Using this modified scaling model, simulations of air showers for primary protons and iron nuclei of different energies have been carried out. The number of hadrons per shower satisfying the selection conditions of run II, called the efficiency factor $\epsilon(E)$ earlier, has been determined from these simulations as discussed in Sec. V. These values of $\epsilon(E)$ for few selected primary energies are compared with values obtained with the scaling model in Fig. 8. It is evident from this figure that the change in ϵ due to these changes in the scaling model is not very significant ($\leq 20\%$). Consequently no significant change is expected in the event rate. Also the delayed fraction for the hadrons in showers generated with the modified scaling model has not changed significantly. These results show that the extent of scaling violation necessary to account for the accelerator data up to $\bar{p}p$-collider energies does not change the results obtained from the present experiment. It can therefore be concluded that the results on primary composition indicating dominance of heavy nuclei at energies $\sim 10^5 - 10^6$ GeV are not dependent sensitively on the model of particle interactions for all practical purposes within the constraints imposed by results available from the new $\bar{p}p$-collider experiments.[9]

B. Nature of delayed hadrons

The simulations have shown that nearly all the hadrons that give 5–20-particle signal in the hadron detector (T_3) and arrive delayed by 15 nsec or greater are nucleons. While very few of these delayed nucleons satisfy the selection conditions of run II in proton showers, more are observable as delayed hadrons in iron-nucleus showers. Since every hadron was tagged during the simulations we find that among the detected delayed hadrons, the surviving primary nucleons, produced nucleons (and antinucleons), and recoil target nucleons are mixed in roughly equal proportion. As is to be expected the lower-energy delayed hadrons are preferentially the target nucleons while the higher-energy ones are one of the other two types. These features of simulated hadrons suggest that the delayed fraction in the present experiment is not very sensitively related to the number of nucleon-antinucleon produced in interactions in the atmosphere, in the sense that a smaller change of 20–30% in the baryon-production cross section would not produce a large change in the delayed fraction. This is significant because the increase in baryon-production cross section above ISR energies is not known, though cosmic-ray experiments[51] suggest an increase with energy. The probability f_N of a secondary particle to be a produced nucleon, assumed in simulations to increase with energy as

$$f_N = 0.0164 \ln(1+0.015\times E_{\text{lab}}) ,$$

becomes as high as 0.12 at an energy of 10^5 GeV. This value is higher than the extrapolations[28] from ISR data. It is to be noted that a smaller value for f_N would decrease the expected delayed fraction therefore requiring a still higher proportion of heavy nuclei in the primary flux.

Several background processes which can, in principle, lead to observation of delayed signals in the hadron detector have been discussed elsewhere.[12] Their estimated contribution to the observed de-

layed fraction is negligible.

VII. CONCLUSIONS

The present study of the hadron component and its temporal structure in air showers of primary energies $\sim 10^5 - 10^6$ GeV has shown that specific selection conditions used in the experiment make the experimental results very sensitive to the composition of primary cosmic rays in this energy range. These selection conditions require that surrounding the detected hadron there should be (i) shower particle density ≥ 18 m^{-2} and (ii) hadronic energy incident over 4 m$^2 \geq 30$ GeV. The experimental results under these conditions are (i) the flux of hadrons giving a signal of ≥ 5 equivalent particles in the detector is 1.85×10^{-7} cm^{-2}sr^{-1}sec^{-1} and (ii) a fraction $(0.55 \pm 0.05)\%$ are delayed by 15 nsec or more.

These results have been compared with results expected from Monte Carlo simulations of air showers using a scaling model for particle interactions and the instrumental response for the hadrons incident over the detector area. This comparison shows that the experimental results cannot be understood in terms of a composition of primary cosmic rays which is similar to that observed at lower energies (≤ 100 GeV/A) by direct experiments. A successful understanding of the observations requires a relative change between the energy spectra of protons (and lighter nuclei) and the heavy nuclei in the energy range $\sim 10^5 - 10^6$ GeV which would make the proportion of iron-group nuclei as large as $40-60\%$ of the primary flux at these energies. We therefore conclude that the composition of cosmic rays is varying with energy in the energy range $\sim 10^4 - 10^8$ GeV: from being dominated by protons and lighter nuclei below 10^4 GeV to becoming dominated by heavy (iron-group) nuclei between 10^5 and 10^7 GeV.

ACKNOWLEDGMENTS

We wish to thank Tom Morrison, Eldon Vann, Ralph Sutton, Harriet Sutton, Geeta Tonwar, Sriram Ramaswamy, Calvin Simpson, and James Schombert for their contribution to various phases of the experiment and data analysis. Discussions with J. Ormes, V. K. Balasubrahmanyan, P. H. Steinberg, S. I. Nikolsky, A. M. Hillas, A. E. Chudakov, V. I. Yakovlev, T. K. Gaisser, and G. A. Snow are gratefully acknowledged. This work was supported in part by the National Science Foundation and the University of Maryland Computer Science Center.

---

*Present address: George Mason University, Fairfax, VA 22030.

†Present address: State University of New York at Stony Brook, Stony Brook, NY 11974.

‡Present address: Pfizer Corp., Columbia, MD.

§Present address: Now at Nuclear Physics Laboratory, Oxford, England.

||Present address: Goddard Space Flight Center, Greenbelt, MD.

¶On leave of absence from Tata Institute of Fundamental Research, Colaba, Bombay, India.

**Present address: Tata Institute of Fundamental Research, Colaba, Bombay, India.

[1]N. L. Grigorov *et al.*, in *Proceedings of the 12th International Conference on Cosmic Rays, Hobart, Tasmania, 1971,* edited by A. G. Fenton and K. B. Fenton (Univ. of Tasmania Press, Hobart, Tasmania, 1971), Vol. 5, p. 1946.

[2]M. Simon *et al.*, Astrophys. J. 239, 712 (1980); V. K. Balasubrahmanyan and J. F. Ormes, *ibid.* 186, 109 (1973); C. D. Orth *et al.*, *ibid.* 226, 1147 (1978).

[3]R. W. Ellsworth *et al.*, Astrophys. Space Sci. 52, 415 (1977).

[4]T. K. Gaisser *et al.*, Rev. Mod. Phys. 50, 859 (1978).

[5]G. B. Yodh, in *Cosmology and Particles,* proceedings of the XVIth Rencontre de Moriond, Les Arcs, France, 1981, edited by J. Trân Thanh Vân (Editions Frontieres, Dreux, France, 1981).

[6]R. P. Feynman, Phys. Rev. Lett. 23, 1415 (1969).

[7]E. Yen, Phys. Rev. D 10, 836 (1974); F. E. Taylor *et al.*, *ibid.* 14, 1217 (1976).

[8]G. B. Khristiansen, in *16th International Cosmic Ray Conference, Kyoto, 1979, Conference Papers* (Institute of Cosmic Ray Research, University of Tokyo, Tokyo, 1979), Vol. 14, p. 360.

[9]G. Arnison *et al.*, Phys. Lett. 107B, 320 (1981); K. Alpgard *et al.*, *ibid.* 107B, 315 (1981).

[10]J. A. Goodman, Ph.D. thesis, University of Maryland, 1978 (unpublished).

[11]J. A. Goodman *et al.*, Phys. Rev. Lett. 42, 854 (1979).

[12]J. A. Goodman *et al.*, Phys. Rev. D 19, 2572 (1979).

[13]F. Siohan *et al.*, J. Phys. G 4, 1169 (1978).

[14]R. W. Ellsworth *et al.*, in *Proceedings of the 15th International Conference on Cosmic Rays, Plovdir, 1977,* edited by B. Betev (Bulgarian Academy of Sciences, Sofia, 1977), Vol. 11, p. 499.

[15]J. R. MacFall *et al.*, J. Phys. G 5, 861 (1979).

[16]J. R. MacFall *et al.*, Nucl. Phys. B151, 213 (1979).

[17]W. V. Jones, Phys. Rev. 187, 1868 (1969); W. V. Jones, private communication.

[18]T. A. Gabriel and B. L. Bishop, Nucl. Instrum. Methods 155, 81 (1978).
[19]M. Holder *et al.*, Nucl. Instrum. Methods 151, 69 (1978).
[20]B. Barish *et al.*, Nucl. Instrum. Methods 116, 413 (1973).
[21]S. C. Tonwar, in *17th International Cosmic Ray Conference, Paris, 1981, Conference Papers* (Centre d'Études Nucleaires, Saclay, 1981); B. V. Sreekantan and S. C. Tonwar, in *16th International Cosmic Ray Conference Kyoto, 1979, Conference Papers* (Ref. 8), Vol. 8, p. 287.
[22]L. W. Jones *et al.*, Phys. Rev. 164, 1584 (1967).
[23]S. C. Tonwar *et al.*, J. Phys. A 4, 868 (1971).
[24]S. C. Tonwar *et al.*, Lett. Nuovo Cimento 1, 531 (1971).
[25]W. Busza *et al.*, Phys. Rev. Lett. 34, 383 (1975).
[26]T. K. Gaisser and G. B. Yodh, Annu. Rev. Nucl. Part. Sci. 30, 475 (1980); S. C. Tonwar, J. Phys. G 5, L193 (1979).
[27]W. Morris *et al.*, Phys. Lett. 56B, 395 (1975).
[28]M. Antinucci *et al.*, Lett. Nuovo Cimento 6, 121 (1973); T. K. Gaisser and F. Halzen, Phys. Rev. D 11, 3157 (1975).
[29]J. R. Johnson *et al.*, Phys. Rev. D 17, 1293 (1978); D. Cutts *et al.*, Phys. Rev. Lett. 40, 141 (1978).
[30]F. W. Busser *et al.*, Phys. Rev. Lett. 46B, 471 (1973).
[31]F. Halzen and J. Luthe, Phys. Lett. 48B, 440 (1978); F. Halzen, Nucl. Phys. B92, 404 (1975).
[32]B. Rossi, *High Energy Particles* (Prentice-Hall, New York, 1952).
[33]A. M. Hillas and J. Lapikens, in *Proceedings of the 15th International Conference on Cosmic Rays, Plovdiv, 1977* (Ref. 14), Vol 8, p. 460.
[34]H. Whiteside *et al.*, Nucl. Instrum. Methods 109, 375 (1973).
[35]S. C. Tonwar and P. R. Viswanath, in *Proceedings of the Xth International Symposium on Multiparticle Dynamics, Goa, India, 1979,* edited by S. N. Ganguli, P. K. Malhotra, and A. Subramanian (Tata Institute, Bombay, 1980), p. 760.
[36]R. H. Vatcha and B. V. Sreekantan, J. Phys. A 6, 1050 (1973).
[37]C. Cezarsky, Ann. Rev. Astron. Astrophys. 18, 289 (1980).
[38]R. Cowsik *et al.*, in *17th International Cosmic Ray Conference, Paris, 1981, Conference Papers* (Ref. 21), Vol. 2, p. 120.
[39]R. Cowsik and M. Wilson, in *Proceedings of the 13th International Conference on Cosmic Rays, Denver, 1973* (Colorado Associated Univ. Press, Boulder, 1973), Vol. 3, p. 500.
[40]B. V. Sreekantan, Rapporteur's paper in *16th International Cosmic Ray Conference, Kyoto, 1979, Conference Papers* (Ref. 8), Vol. 14, p. 345.
[41]G. W. Mason *et al.*, in *Proceedings of the 14th International Conference on Cosmic Rays, Munich, 1975,* edited by Klaus Pinkau (Max-Planck Institut, München, 1975), Vol 8, p. 2943. M. Deakyne *et al.*, in *Cosmic Rays and Particle Physics—1978,* proceedings of the Bartol Conference, edited by T. K. Gaisser (AIP, New York, 1979); A. E. Chudakov *et al.*, in *16th International Cosmic Ray Conference, Kyoto, 1979, Conference Papers* (Ref. 8), Vol. 10, p. 188.
[42]For example, J. W. Elbert *et al.*, Phys. Rev. D 12, 660 (1975) and J. W. Elbert, private communication (1981).
[43]N. N. Kalmykov *et al.*, in *Proceedings of the 14th International Conference on Cosmic Rays, Munich, 1975* (Ref. 41), Vol. 8, p. 2861. J. Olejniczak *et al.*, J. Phys. G 3, 847 (1977).
[44]B. S. Acharya *et al.*, in *16th International Cosmic Ray Conference, Kyoto, 1979, Conference Papers* (Ref. 8), Vol. 13, p. 272.
[45]B. S. Acharya *et al.*, in *17th International Cosmic Ray Conference, Paris, 1981, Conference Papers* (Ref. 21).
[46]B. A. Khrenov *et al.*, in *16th International Cosmic Ray Conference, Kyoto, 1979 Conference Papers* (Ref. 8), Vol. 8, p. 351. N. V. Grishina *et al.*, in *17th International Cosmic Ray Conference, Paris, 1981, Conference Papers* (Ref. 21), Vol. 6, p. 3.
[47]K. Kamata, in *17th International Cosmic Ray Conference, Paris, 1981, Conference Papers* (Ref. 21).
[48]S. I. Nikolsky, in *Proceedings of the 15th International Conference on Cosmic Rays, Plovdiv, 1977* (Ref. 14), Vol. 10, p. 290.
[49]A. M. Hillas, in *16th International Cosmic Ray Conference, Kyoto, 1979, Conference papers* (Ref. 8), Vol. 6, p. 13; Vol. 9, p. 13.
[50]R. W. Ellsworth, in *16th International Cosmic Ray Conference, Kyoto, 1979, Conference Papers* (Ref. 8), Vol. 7, p. 333.
[51]S. C. Tonwar, in *Proton-Antiproton Collider Physics—1981,* proceedings of the Workshop on Forward Collider Physics, Madison, Wisconsin, edited by V. Barger, D. Cline, and F. Halzen (AIP, New York, to be published).